CNES Studies of On-Board Compression for Multispectral and Hyperspectral Images

Carole Thiebaut*[a], Emmanuel Christophe[a], Dimitri Lebedeff[b], Christophe Latry[a]
[a]CNES, France, [b]Thales Alenia Space, France
carole.thiebaut@cnes.fr

ABSTRACT

Future high resolution instruments planned by CNES for space remote sensing missions will lead to higher bit rates because of the increase in resolution, dynamic range and number of spectral channels for multispectral (up to 16 bands) and hyperspectral (hundreds of bands) imagery. Lossy data compression is then needed, with compression ratio goals always higher and with low-complexity algorithm. For optimum compression performance of such data, algorithms must exploit both spectral and spatial correlation. In the case of multispectral images, CNES (in cooperation with Thales Alenia Space, hereafter TAS) studies have led to an algorithm using a fixed transform to decorrelate the spectral bands, the CCSDS codec compresses each decorrelated band using a suitable multispectral rate allocation procedure. This low-complexity decorrelator is adapted to hardware implementation on-board satellite and is under development. In the case of hyperspectral images, CNES (in cooperation with TAS/TeSA/ONERA) studies have led to a full wavelet compression system followed by zerotree coding methods adapted to this decomposition. We are investigating other preprocessors such as Independent Component Analysis which could be used in both approaches. CNES also participates to the new CCSDS Multispectral and Hyperspectral Data Compression Working Group.

Keywords: compression, satellite images, multispectral, hyperspectral.

1 INTRODUCTION

On-board image compression for space missions is considered nowadays as a very powerful tool to optimize on-board resources needed to store and transmit image data to ground. Compression will be more and more useful because of future high resolution instruments planned by CNES which will have higher number of spectral channels than current instruments. In the case of so-called multi-spectral or super-spectral mission about ten bands are acquired simultaneously with a narrow swath and a spatial resolution from 10m to 1km, like the French-Israelian VENμS mission (12 bands from visible to near infra-red, spatial resolution between 10 and 20m, swath equal to 27,5km, launch date in 2009), the ESA GMES Sentinel 2 mission (18 bands, spatial resolution 5m, swath larger than 200 km) or the imager of Meteosat Third Generation (5 bands, spatial resolution 500m). In this case, lossy compression is not always necessary because of the small amount of data induced by small swath but lossless compression ratio could be improved by considering the spectral correlation. In the case of very high resolution instruments, a smaller number of bands are acquired, typically 4 bands: the blue (not for SPOT5), red, green and near infra-red, sometimes completed with the short-wave infrared or a panchromatic band with a better spatial resolution. This is the case for the SPOT5 instrument launched in 2002 (spatial resolution 10m for multispectral bands) and the PLEIADES one to be launched in 2009 (spatial resolution 2.8m for multispectral bands). For this type of instrument, the data rate is very high and data compression is mandatory. The more images can be compressed, the best it is for the mission because a higher number of images can be acquired and transmitted to ground, and a smaller mass memory is also needed. Up to now, data compression is done independently on each channel, meaning, on the panchromatic one and on each multispectral channel. In this case, the so-called "monospectral" compressor exploits only the spatial redundancies of the image, ignoring the redundancy between the different images of the same scene taken in different spectral bands. This is the case for both satellites cited above which do not have on-board spectral correlation compression.

In the "multispectral compression" study, CNES and TAS goal was to define a low complexity and flexible fixed rate compression algorithm suited for multispectral missions. Moreover, in order to reduce the development costs, the proposed algorithm had to re-use, as far as possible, already existing compressors, such as CNES algorithms already used in previous missions or standard algorithms suited for space missions [1]. The proposed algorithm is then composed of a decorrelation stage which can be used in front of existing monospectral compressors.

*carole.thiebaut@cnes.fr; phone 33 561 283 404; fax 33 561 281 996

Hyperspectral imagery is a noticeably different framework for CNES which has not planned any hyperspectral mission up to now, even if some instrument concepts are under study for future missions. However, airborne hyperspectral data have been available since the early 1990s (AVIRIS), and their applications for geological, agricultural or military purposes are well established. Later, in 2000, spaceborne hyperspectral data became available with the launch of Hyperion by NASA. These sensors collect the spectrum for each pixel of the image. Typically, hyperspectral images comprise hundreds of narrow and contiguously bands from 0.4 to 2.5 micrometers. Hyperspectral sensors (also called imaging spectrometers) could be used but compression of this kind of data is mandatory in order to avoid on-board band selection such as MERIS or MODIS instruments. Because hyperspectral imagery appears to be of a growing interest and also to anticipate the problem of compression if CNES decides to use one of these sensors, CNES has led a deep investigation in this technique through a PhD Thesis on "hyperspectral compression and the definition of quality criteria for this kind of data" [2].

For both studies, CNES has decided to consider a pre-processing stage decorrelation of the spectral axis, as it is done in JPEG2000 standard for multicomponent transform [3, 4]. But multispectral and hyperspectral data do not have the same spectral characteristics. We have observed that hyperspectral data have long distance correlation as shown in Figure 1 which implies that the decorrelator used for this kind of data should be different from the one used for multispectral data. In the "multispectral compression" study, the pre-processor is based on a Karhunen-Loeve Transform (KLT) and in the "hyperspectral compression" study, a Discrete Wavelet Transform (DWT) is used. To complete these two studies, CNES started recently a new study with a third team on the use of Independent Component Analysis (ICA) for multispectral and hyperspectral data. This study will provide comparative performances with other two studies on each type of data. The preliminary results of this transform are presented here.

CNES choices of pre-processor have been made according to several points which will be exposed in Section 2. Those choices depend on performances but also on implementation complexity considerations such as limited resources (moreover if it is a hardware implementation) and a limited memory. For high data rate instruments, compression is often performed in hardware, meaning rad-tolerant FPGA or ASIC. The CNES studied algorithms should be suited to this kind of implementation. Other compression techniques adapted to on-board hyperspectral data (low-complexity) are known: in [5], lossless compression is performed by a predictive method and in [6], Vector Quantization is used.

The spatial compression is always performed with the discrete wavelet transform (DWT) used in the JPEG2000 and CCSDS standards [7]. CNES belongs to the CCSDS data compression group and was involved in lossless and lossy data compression recommendations. It is still active in the latest group which deals with Multispectral and Hyperspectral Data Compression. CNES was also very active in JPEG2000 standard group during the algorithm development. The coding stage depends on the decorrelation transform. For multispectral images using KLT, a coding of the decorrelated bands is performed with the CCSDS standard compressor; for hyperspectral data, an integrated coding algorithm of the decorrelated data was chosen. The used methodologies are described in Section 2. The algorithms have been studied by different teams and at different times. Comparative studies on same scenes have not been done yet. A brief description of the test data for both types of images is given in Section 3. Final results of each algorithm are illustrated in Section 4. Last Section is devoted to conclusions and presentation of future works.

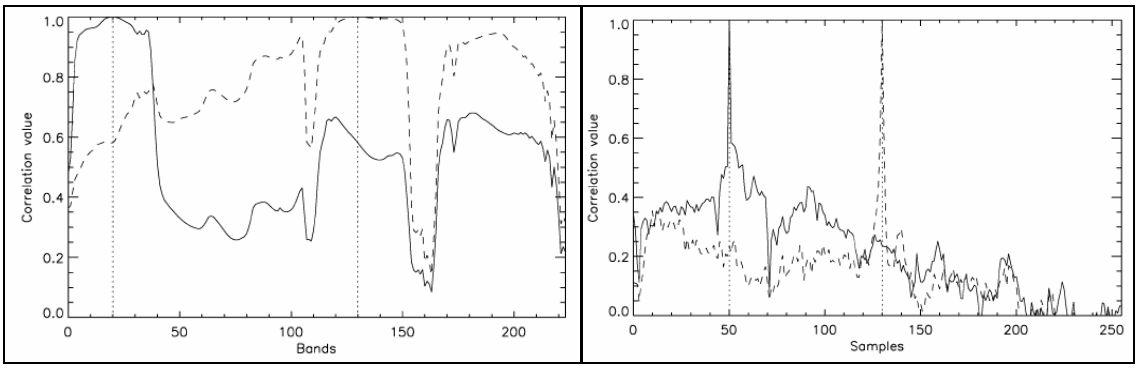

Figure 1: Left - Spectral correlation coefficient between band 20 and other bands (solid line) and band 130 and the other bands (dashed line). Right - Spatial correlation coefficient between sample 50 and other samples (solid line) and sample 130 and the other samples (dashed line).

2 METHODOLOGY

2.1 Introduction

To take the spectral correlation into account, it is possible to use a transform adapted to data characteristics along this axis. For multispectral images (low number of bands), it depends on the spectral range of each band, e.g. if the spectral overlapping is high, the redundancy will be higher. To perform the decorrelation of these data, KLT and ICA have been tested and are presented in the following sections. The advantages of these transforms are their performances and their power of decorrelation which is theoretically the optimal. But their drawbacks are that they are signal-dependent and need to be computed for each image. To reduce the on-board complexity of the transform, fixed matrices have been computed.

For hyperspectral images, the spectral resolution is very narrow and constant but the spectral profile of each spatial pixel is very important for applications meaning that degradation induced by compression should be less important in this axis than in spatial one. Moreover, as previously said, the correlation that appears in the spectral dimension between two distant bands (Figure 1) is completely different from the short-range correlation in spatial dimensions. The correlation may remain significant even if the distance between bands increases, e.g., correlation coefficient between bands 20 and 180 is greater than 0.6. The correlation between samples (i.e. in the spatial dimension) drops sharply as the distance increases: with a distance greater than ten samples, the correlation coefficient is below 0.4. To perform the decorrelation of these data, DWT and ICA have been tested and are presented in the following sections.

Compression performances using DCT, KLT or DWT spectral decorrelation are compared in Figure 2 for a hyperspectral image (Moffet/AVIRIS). The PSNR criterion is shown for several bit rates. As expected, introducing a decorrelation prior to JPEG 2000 coder greatly improves the results.

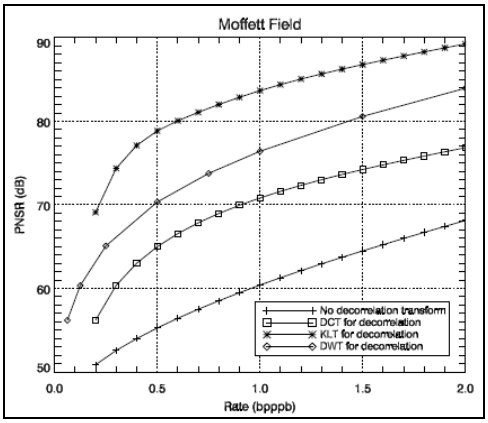

Figure 2: Performances of JPEG2000 codec without interband decorrelation or using DCT, KLT and DWT.

2.2 KLT for multispectral data

The multispectral algorithm is based on previous studies [8] made by CNES and TAS. The decorrelation stage was performed by a KLT on spectral channels. The choice of this transform is justified by several reasons: transform decorrelation performs better than a predictive method. A transform specifically suited for spectral application was not known to the authors, the KLT is the optimal transform (considering order 2 decorrelation) and the KLT complexity in multispectral case is compliant with the algorithm constraints. We have proposed a decorrelation stage based: either on a fixed transform evaluated previously on a set of images or on the KLT locally adapted to the studied block, implemented in a scan-based mode as previously proposed in [1]. For high compression levels, visual artifacts appear because the locally adapted transform induces contrast variations. The choice between both decorrelation options has been done after performance comparisons, a complexity analysis [1] and a hardware architecture analysis. Only the fixed transform is kept for future studies because of: the performances obtained with this transform which are very good and nearly optimal, the absence of the visual discontinuity artifact, the drop in complexity and finally the absence of auxiliary data (coming from KLT matrices) which means less overhead data.

An on-board registration algorithm and its implementation complexity are studied. We also analyze the effect of the non-registration between spectral bands on the performances by simulating non-registered images. The following section describes the proposed algorithm.

2.2.1 Spectral decorrelation by a fixed transform

The optimal transform (locally adapted) was given up because of its complexity and the artifacts it produced. Fixed spectral transform, dedicated to the corresponding sensor, has shown a relatively low sensibility with regards to scene variations. Different types of data (i.e. sensor) have been considered. For Quickbird, 4 bands multispectral images of size around 6000 x 6000 pixels on various scenes spread all over the world have been used in order to compute the fixed KLT matrix. The algorithm is the one presented in [1]; the block diagram is reminded in Figure 3. The bit rate allocation procedure and the converting stages are presented below.

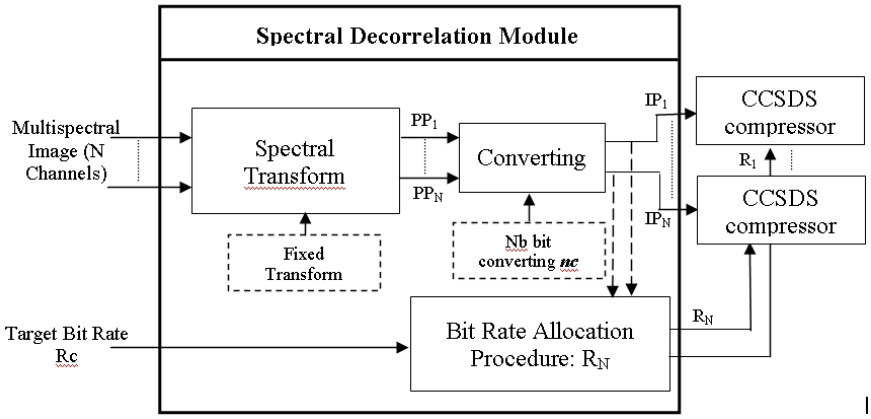

Figure 3: Multispectral compression block-diagram.

2.2.2 Converting stage

Because the eigen-planes are computed in a floating point format, they must be converted in so-called eigen-images to be analyzed by compressors. It has been shown that the theoretical maximum absolute value is given by $N^{1/2}.2^{nbit\_input}$ where *nbit_input* is the dynamic range of the input image and N the number of spectral bands. In the case of CCSDS codec, a conversion on 16 bits is realized. The impact of this conversion is negligible.

2.2.3 Rate allocation procedure: new algorithm

In previous works, an already existing CNES compressor was used (MR-CNES), and in particular, the rate allocation procedure of this algorithm [8]. This procedure allows reaching the targeted bit rate for each compression test. This procedure uses the hypothesis that the subbands probability density functions may be modeled by Generalized Gaussians functions. It assigns the rate between 10 subbands and computes the corresponding quantization step size according to the minimization of the Root Mean Square Error. In the multispectral case, the number of considered subbands was extended to Nx10, N being the number of spectral bands. This procedure is very complex and its main drawback is to have the wavelet transformed coefficients at one's disposal, which is not the case with the CCSDS codec as with other well-known codecs. In order to allocate data rate to different bands without having this information but knowing only the original bands, a new rate allocation procedure has been implemented and tested on several images. This procedure is based on the distribution of the complexity criteria of each band or more precisely on each part of image according to the distribution of the data rate of this part of image. The complexity CL (meaning line complexity) of an image is defined as the sum of the absolute value of the difference of each pair of neighbour pixels:

$$CL = \frac{\sum_{i=1}^{n_l} \sum_{j=1}^{n_c - 1} \left| p_{i,j} - p_{i,j+1} \right|}{n_c \times n_l}$$

Using the MR-CNES rate allocation procedure, rate/complexity curves have been plotted and a law has been found for each bit rate. An example for bit rate 2.22 is given in Figure 4 for all 17 QuickBird images. This law is used to compute the bit rate of a channel according to the complexity of its data. Because the CCSDS compressor allows a rate allocation which may vary in the image, this allocation procedure is done for each block of lines, typically 16 lines blocks for our test images. Thus, every 16 lines, 4 bit rates (one for each channel) are computed. This rate allocation procedure is well adapted to on-board computation because it is not complex. It was observed that most energetic bands after KLT have the biggest complexity distribution values (right hand side points cloud) and, on the contrary, lower energy bands have the smallest values (left hand side points cloud).

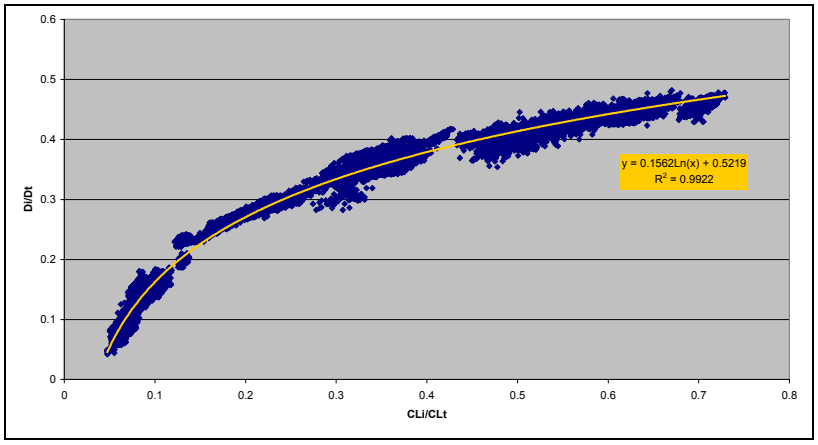

Figure 4: Distribution of the bit rate according to the distribution of the complexity at 2.22 bit/pixel for all QuickBird images. The law associated to this distribution is 0.1562ln(x)+0.5219.

Because the decorrelation stage is a complex thing to perform in hardware implementation, we have also analysed a mode without decorrelation but only with the rate allocation procedure presented above. When applying this procedure to the spectral bands, the bit rate allocated to each channel is not the same because spectral bands do not have the same characteristics. In this case, we use different laws of distribution.

2.2.4 Spatial decorrelation and Coding stage

Each eigen-image from spectral decorrelation and converting stages is compressed with the CCSDS compressor [7], meaning that DWT and CCSDS bit plane encoding are performed for each spectrally decorrelated band. The bit rates obtained by the rate allocation procedure defined above are used and those rates vary every 16 lines and for each spectral band. The decorrelated images are coded on 16 bits after the converting stage, which is a dynamic accepted by the CCSDS compressor. Results presented in Section 4 are obtained with all the modules defined previously.

2.3 Discrete Wavelet Transform for hyperspectral data

2.3.1 Pre-processing stage: DWT

The DWT is a very powerful tool for decorrelating data and for performing a coding of the coefficients. It is used in compression recommendations such as JPEG2000 and CCSDS standards. It is not suited to multispectral data because of the small number of bands but could be useful for hyperspectral data. Moreover, this transform is fixed and not data-dependent which is better for on-board computation. The number of levels of decomposition will be adapted to the number of spectral bands and the complexity of the algorithm.

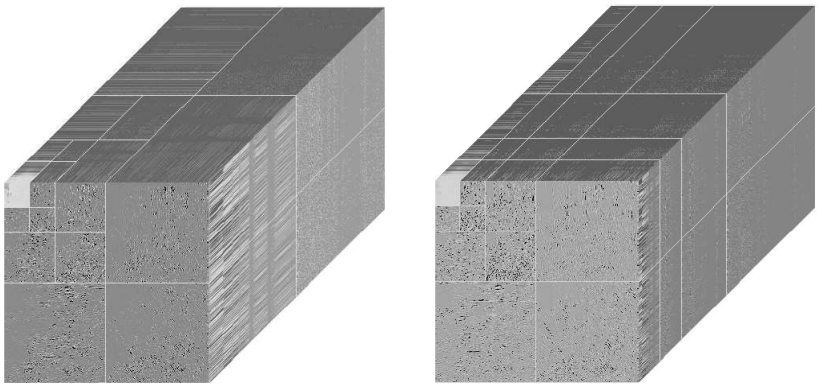

Figure 5: Left – Isotropic wavelet decomposition of a hyperspectral image. Right – Anisotropic wavelet decomposition of a hyperspectral image. For both decompositions, three levels are used.

The fixed transform is obtained by firstly decomposing the spectra with a 1D multiresolution wavelet and then using the standard multiresolution decomposition on the components of the spectral axis. This transform is presented in Figure 5 and is compared to the isotropic one which is often used for volumetric images such as medical MR or CT. In this figure, it can be seen that an important correlation between wavelet coefficients remains in the lower spectral and spatial frequencies (lines of coefficients of the same value). This correlation seems to be less important with the anisotropic decomposition.

After having analyzed the best anisotropic wavelet decomposition in a rate-distortion sense by using the Shoham and Gersho theory [9], we have found that a fixed anisotropic transform performs almost as well as the optimal one found by the best basis analysis (see Figure 6). By choosing a fixed transform, as previously with the KLT study, drawbacks of processing cost and dependency to the image are avoided.

This fixed anisotropic decomposition is suited to on-board satellite implementation because it is the same one as this used for spatial domain. However, for spatial domain, we compute the DWT only on a limited height of the image because of the memory constraints. In perspective of this analysis, a complexity analysis of the 1D DWT in the spectra domain we should performed.

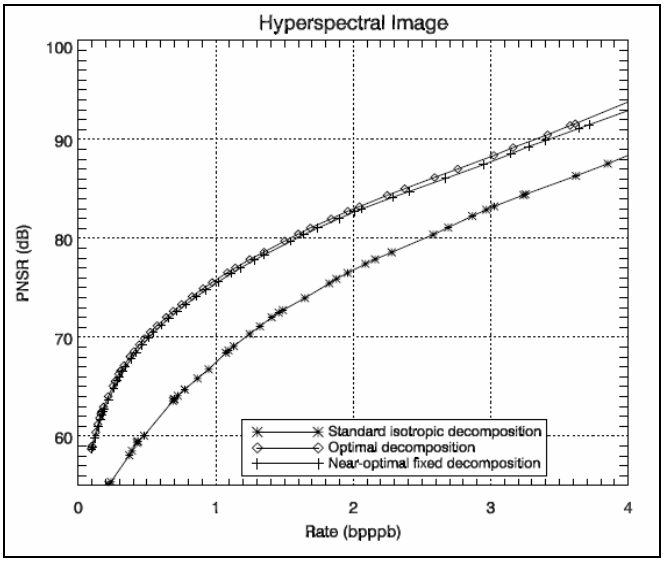

Figure 6: Performances of the standard isotropic, optimal (found by best decomposition analysis) and fixed decompositions on hyperspectral image. Results are obtained with Kakadu software for JPEG2000 implementation.

2.3.2 Coding stage: zero-tree algorithms

Results presented in Figure 6 have been obtained with the JPEG2000 standard (by the use of Kakadu software [10]). A more performing coding procedure has been implemented. This procedure is based on EZW and SPIHT methodologies and performs the coding of zero-trees of coefficients obtained by DWT in spectral axis and DWT in spatial domain [2]. Spatial, spectral and 3D trees were analyzed and an arithmetic coder could be added or not. A statistical study on the proportion of zero-trees was made on the different structures, leading to the choice of a 3D tree (see Figure 7). With a low complexity, EZW manages to give performance similar to those given by JPEG 2000, while providing a fully embedded bitstream. SPIHT performs well, even if used without arithmetic coder. These properties are particularly appealing for the on-board processing of hyperspectral images on space systems. Improvement is still possible, particularly in the case of the SPIHT coder. Making full use of the double linked tree structure or adding an adapted arithmetic coder would yield improved results.

The rate allocation procedure is done implicitly by cutting the resulting bitstream at the targeted bit rate.

Other functionalities have been added in the algorithm, such as the Random Access to the bitstream and resolution scalability [11]. These tools are useful for transmission of lower number of bands or region of interest in the scene.

Some complexity simplifications are also possible, to enable parallel coding. It has be illustrated in [12] for the case of the 3D-EZW with the unconventional use of unsigned binary digit coding.

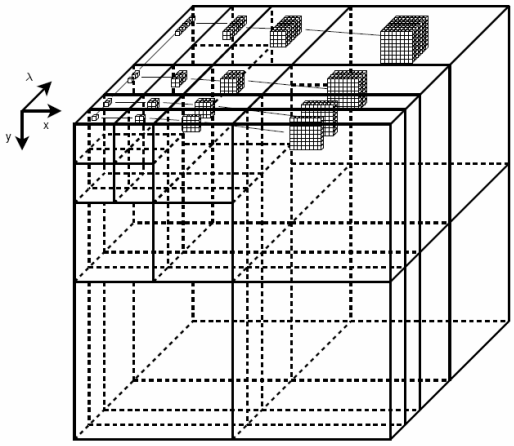

Figure 7: Illustration of the tree structure

2.4 Independent Component Analysis for both types of data

2.4.1 Pre-processing: ICA on spectral bands

High resolution quantization theory shows that the Karhunen-Loeve transform (KLT) is optimal for Gaussian sources. Recently, Narozny et al [13] proposed a new viewpoint in variable high-rate transform coding. They showed that the problem of finding the optimal 1-D linear block transform for a high-rate transform coding system employing entropy constrained uniform quantization may be viewed as a modified ICA problem. This result applies without the presumption of Gaussianity or orthogonality. New algorithms of ICA (ICA_{opt} and ICA_{orth}) were proposed to compute optimal transform for image coding, one for optimal linear transform and one for optimal orthogonal transform. These algorithms are both derived from an algorithm by D. T. Pham that minimizes the mutual information of the transformed components [14]. They were tested on well-known gray-scale images and their performances were comparable to JPEG2000 codec while providing better visual quality. After Narozny has shown the link between ICA and transform coding, Akam-Bita applied and adapted these algorithms on multispectral and hyperspectral satellite images [15]. The procedure is almost the same as for the DWT or the KLT: the ICA transform is performed on the spectral axis and the obtained images are independent from each other. The slight difference is that 2D-DWT can be performed on each band before or after ICA. Both schemes have been analyzed (ICA before DWT and vice-versa) and it has been proven that performances are close for both cases. Figure 8 is the resulting transformed images of a PLEIADES-HR simulated image for KLT and ICA decorrelators. KLT results are ordered by decreasing energy.

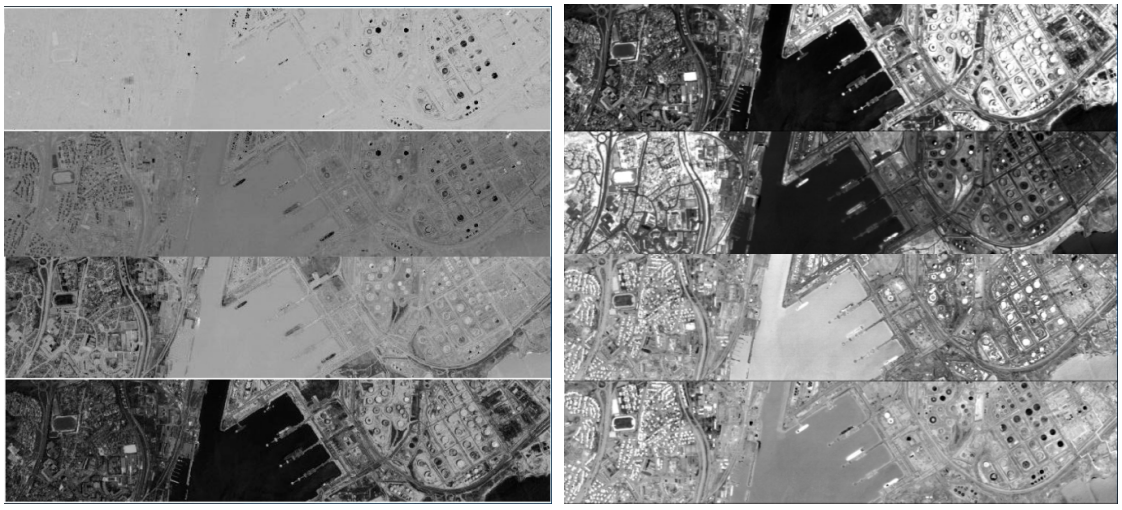

Figure 8: Decorrelated images after ICA (left) and KLT (right) for a PLEIADES-HR simulated image.

2.4.2 Coding stage: on-going work

For the moment, the JPEG2000 standard is used (The Verification Model [16]) for performance analyses. ICA matrix is performed on wavelet coefficients first, outside JPEG2000 coding procedure, and then, ICA matrix is used as the multicomponent transform by JPEG2000. The rate allocation procedure is the one of JPEG2000.

An on-going study will lead to the development of a coding algorithm suited to the transformed coefficients after ICA on spectral axis and DWT on spatial one. We look forward to performing a zero-tree coding of these coefficients as for the DWT for hyperspectral. Statistical properties on the proportion of zero-trees are analyzed. They will lead to tree building and to adaptation of EZW and SPIHT algorithm for both multi and hyperspectral data. Moreover, a fixed transform such as the KLT study, is under development, one for multispectral case and one for hyperspectral. The main drawback of ICA is the computation cost which is very high to find the transform matrix. In perspective of this work, the complexity of this transform will be estimated.

3 DATA

3.1 Multispectral images

Different types of data were used for the performance evaluation: simulated PLEIADES-HR images fully representative simulations using very high resolution airborne data, QuickBird images and SPOT 5 images (see Table 1).

Table 1: Test images characteristics

	PLEIADES	QuickBird	SPOT 5
Spectral Bands	B0 [450-530nm] B1 [510-590nm] B2 [620-700nm] B3 [775-915nm]	B0 [450-520nm] B1 [520-600nm] B2 [630-690nm] B3 [760-900nm]	 B1 [500-590nm] B2 [610-680nm] B3 [780-890nm]
Pixel Resolution (XS bands)	2.8 m	2.44 m	10 m
Dynamic input range	12 bits	11 bits	8 bits
MTF at Nyquist Frequency (XS)	~0.35	Between 0.25 and 0.4	~0.35
SNR at middle range radiance	~130	-	~200

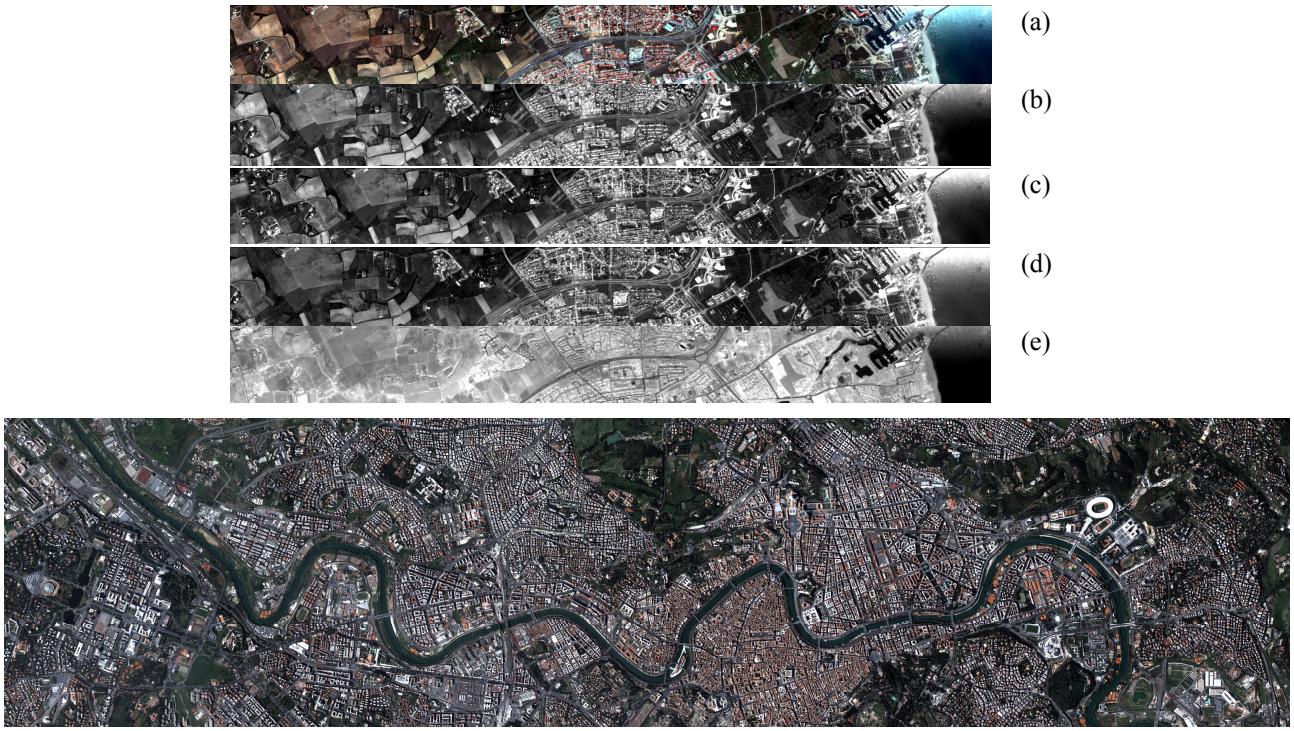

Figure 9: Multispectral image examples. Top Panel – Perpignan/PLEIADES-HR simulated image in RGB mode (a), blue band (b), green band (c), red band (d) and near infra-red band (e). Down Panel – Rome/QuickBird image in RGB mode.

Figure 9 shows some examples of multispectral images used for performance evaluation. The Perpignan/PLEIADES image has 224 columns, 3928 lines and 4 spectral bands. Rome/QuickBird image has 1496 columns, 6000 lines and 4 spectral bands. They have been turned for presentation.

3.2 Hyperspectral images

Some of the hyperspectral data set images used for experiments are presented in Figures 10 and 11. The set is composed by data from the AVIRIS hyperspectral sensor from JPL/NASA and from the NASA: Hyperion satellite sensor.

The chosen images come from the Moffett Field, Jasper Ridge, Hawaii, Cuprite and Harvard sites. The data for Moffett Field is from the AVIRIS run f970620t01p02 r03 sc03. Two spatial subsets of 256 × 256 pixels are extracted with all the 224 spectral bands. The first one presents uniform spatial area with strong spectral features and the second one is mixed area with city (strong spatial frequency features). Harvard site contains mostly vegetation. First Hawaii site presents two areas (mineral and sea) delimited by a coast line and the second site illustrates a run containing clouds thus a higher dynamic level and strong contrasts. Hyperion image covers Moffett field area with a different sensor (cf Figure 10).

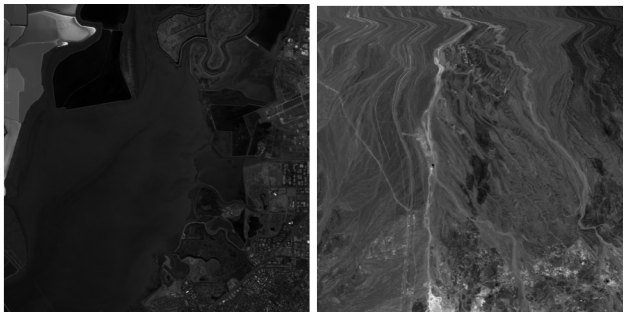

Figure 10: Moffett and Cuprite images from AVIRIS sensor: 512x512 pixels and 224 bands.

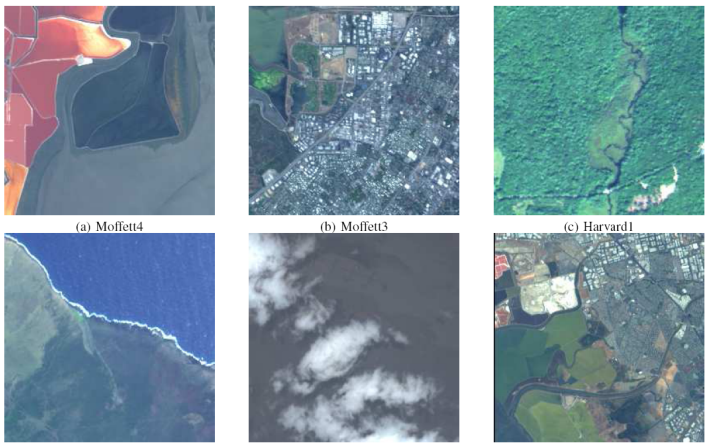

Figure 11: Hyperspectral images used for experiments: (a) and (b) are different parts from the f970620t01p02 r03 run from AVIRIS sensor on Moffett Field site. (c) is from the f010903t01p01 r03 AVIRIS run over Harvard Forest (d) and (e) are from f000414t01p03 r08 run over Hawaii. (f) is from Hyperion space sensor (EO1H0440342002212110PY)

4 RESULTS

In this section, several performance results are presented. For clarity, not all the results are exposed. The reader should refer to the different related papers. Because these studies have been performed by three different teams, the results for ICA, DWT and KLT can not be given for the same scenes and can not be compared. However, ICA is compared with KLT (not the fixed one developed for on-board computation), and DWT with the JPEG2000 component transform. Section 4.1 is devoted to definition of some quality criteria.

4.1 Multispectral quality criteria definition

Considering f_0 as the pixel intensity of the original image and f_r pixel intensity of the decompressed image, the computed quality criteria are defined below:

- Root Mean Square Error (RMSE): $\mathrm{RMSE} = \sqrt{\frac{1}{M.N}\sum_{i=1}^{N}\sum_{j=1}^{M}\left[f_0(i,j) - f_r(i,j)\right]^2}$

- Peak Signal to Noise Ratio (PSNR): $\mathrm{PSNR}_{dB} = 20\log_{10}\left\{\frac{2^{\mathrm{input\_dynamic\_range}} - 1}{\mathrm{RMSE}}\right\}$

- Maximum Error (Emax): $\mathrm{Emax} = \mathrm{MAX}_{i,j}\left|f_0(i,j) - f_r(i,j)\right|$

These criteria are computed for each spectral band. Others criteria such as the NDVI should also be computed because they are close to the application.

4.2 Hyperspectral quality criteria definition

In [17], 15 quality criteria have been studied for classification applications of hyperspectral data. A set of five criteria was defined to characterize the nature and the level of the degradation affecting an image and to predict the performance of a given application. A set of criteria is more relevant than only just one criterion, because each one has a different sensitivity to different image degradations. The five criteria, namely, RRMSE, MAE, $Q_{(x,y)}$, F_λ, and Emax can be computed on each hyperspectral image to give an accurate estimation of the nature of the degradation and of their intensity. These statistical criteria are defined in [17]. We do not list them here.

4.3 Results for Multispectral Data

4.3.1 Fixed KLT results

For multispectral compressor based on KLT, performance evaluation conditions consist in testing three values of data rate: 1.67 bpp, 2.22 bpp and 3.33 bpp. The number of lines considered for the rate allocation procedure is 16 lines. The CCSDS compressor [7] is the one from GSFC: CCSDS Image Data Compression Simulation Software, 25 April 2006 (V2.0.3), NASA's Goddard Space Flight Center.

Compression of each spectral band is performed independently with a CNES compressor called MR-CNES [8]. Performances of independent compression and those of the proposed algorithm with fixed KLT before CCSDS codec are compared. Figure 12 presents the PSNR criterion at 1,67 and 2,22 bpp for Rome/QuickBird (1496x6000 pixels, 4 bands) and Montpellier/PLEIADES (2456x224 pixels, 4 bands) images. It is shown that a systematic gain is obtained in multispectral case compared to monospectral compression. Moreover, image quality is stabilized over all spectral bands with the multispectral compression. This observation was systematic for all test images and for all three sensors, even in the case of non-registered bands.

A model representative of the hardware implementation (FPGA) of the proposed algorithm was performed. This implementation will perform decorrelation, converting and rate allocation procedure stages. Results of the so-called quantized model are presented in Figure 13. Performances are very close to the real algorithm.

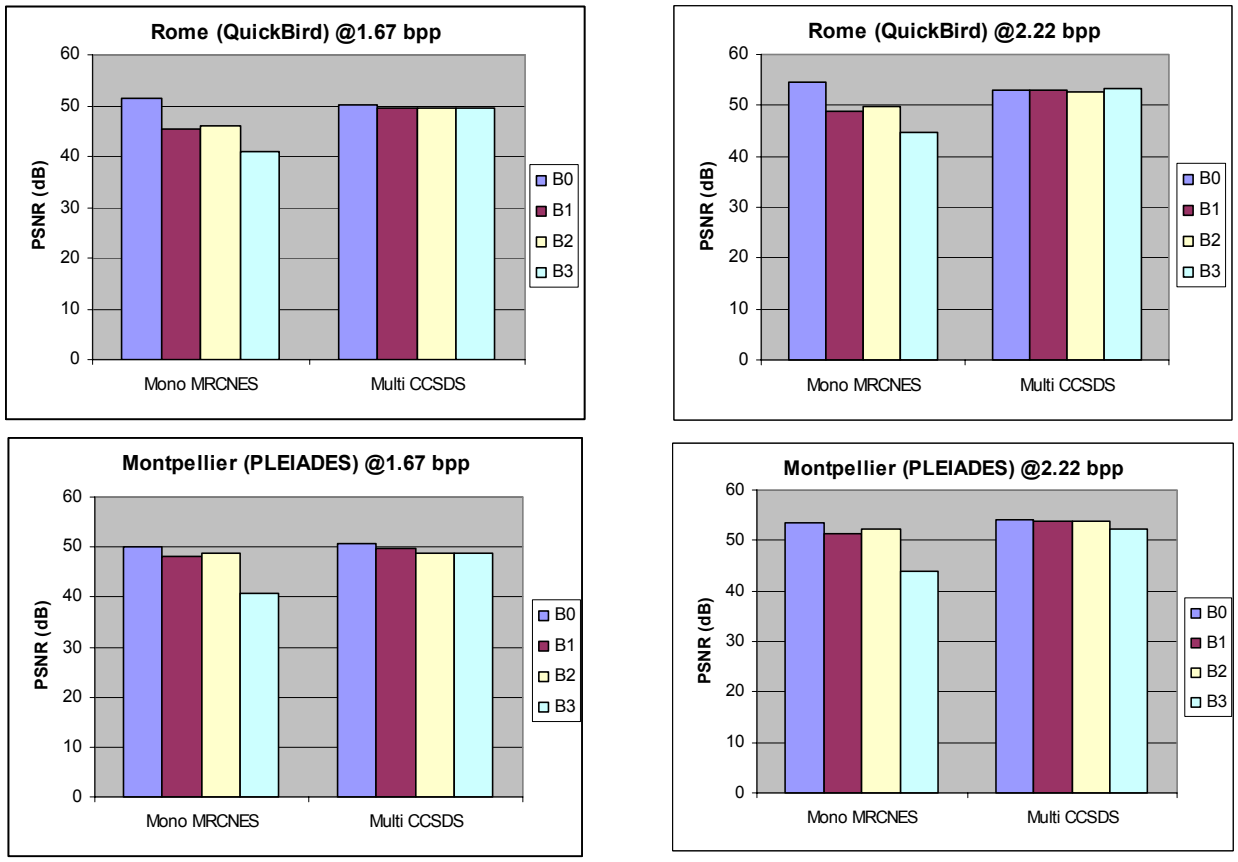

Figure 12: Performances of the fixed KLT transform associated with the CCSDS compressor on some test images. Mono MRCNES means compression of each band independently. Multi CCSDS is the proposed compressor. Results are shown at 1.67 and 2.22 bit/pixel.

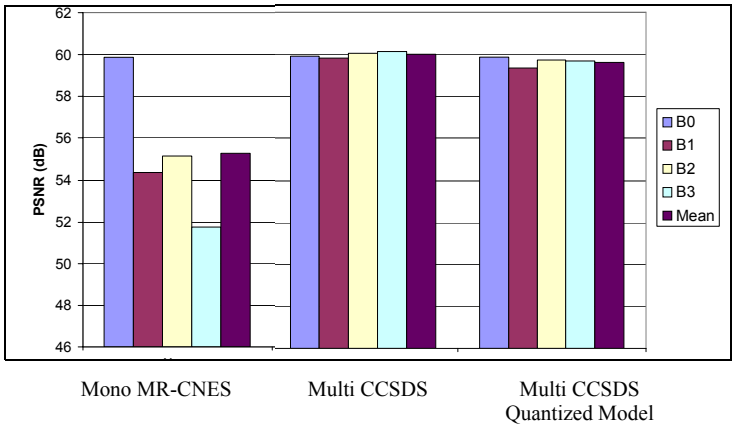

Figure 13: Left - Performances of the compression of each band independently. Middle – Performances of the proposed compressor. Right – Performances of the quantized model of the proposed compressor.

4.3.2 ICA results

ICA results are performed for both ICA modified algorithms called ICA_{orth} and ICA_{opt} and are compared with the KLT (not the same as the one presented above). These transforms are used as the multicomponent transform in JPEG2000 codec. For clarity, only one example for multispectral case is given. PSNR criterion for Vannes/PLEIADES image is presented Figure 14. KLT and ICA results are very close to each other for all tested multispectral images. On some of them like Vannes/PLEIADES, both ICA algorithms over-perform KLT (see Table 2) but for other scenes such as Montpellier/PLEIADES, it is the reverse situation. Both ICA algorithms perform nearly the same for all test images.

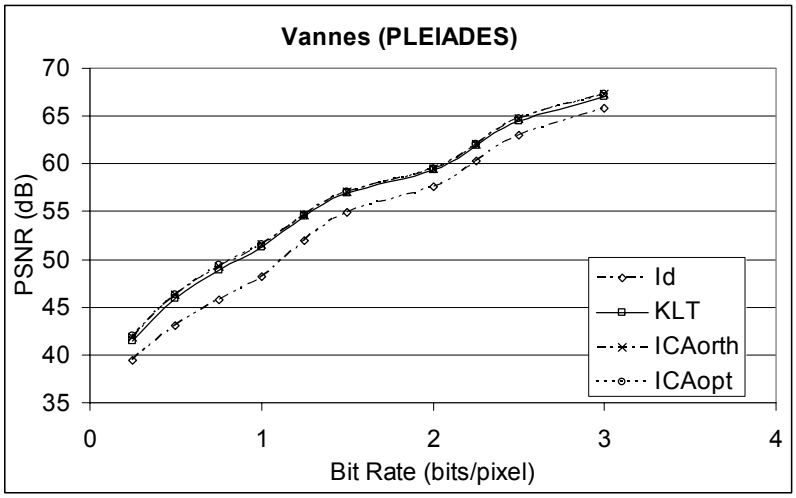

Figure 14: Performances of both ICA algorithms compared to KLT and Identity (no decorrelation) for Vannes/PLEIADES image (3736x352 pixels) for various bit rates.

Table 2: PSNR difference values between ICA algorithms and KLT in dB for each targeted bit rate presented in Figure 14.

Bit Rate (bpp)	**0.25**	**0.5**	**0.75**	**1**	**1.25**	**1.5**	**2**	**2.25**	**2.5**	**3**
ICAorth-KLT	*0.41*	*0.44*	*0.37*	*0.31*	*0.2*	*0.17*	*0.22*	*0.22*	*0.21*	*0.21*
ICAopt-KLT	*0.46*	*0.52*	*0.44*	*0.36*	*0.21*	*0.18*	*0.22*	*0.22*	*0.21*	*0.2*

4.4 Results for Hyperspectral Data

4.4.1 DWT results

All results are available in references [2], [9], [11] and [12]. Here, we only show one example of performance (PSNR criterion) of the algorithms: 3D-EZW and 3D-SPIHT, with or without arithmetic coding, compared to JPEG2000 standard on Moffett image (Figure 15). Without arithmetic coder, SPIHT is better than EZW. But with the arithmetic coder, the gain for SPIHT is not as important as for EZW. This is due to the fact that the output of SPIHT is binary. With a lower complexity than JPEG2000 algorithm, EZW provides very similar PSNR and even outperforms JPEG2000 for low bit rates. The advantage of both modified EZW and SPIHT algorithms is their hierarchically organized bitstream allowing decompression at several bit rates from only one compressed bitstream. For JPEG2000, every curve point needs a complete re-computation of compression stage to reach the targeted bit rate. Moreover, the global rate allocation procedure performed by JPEG2000 is very complex (Lagrangian optimization) and prevents spatial hardware implementation of this standard with current technologies.

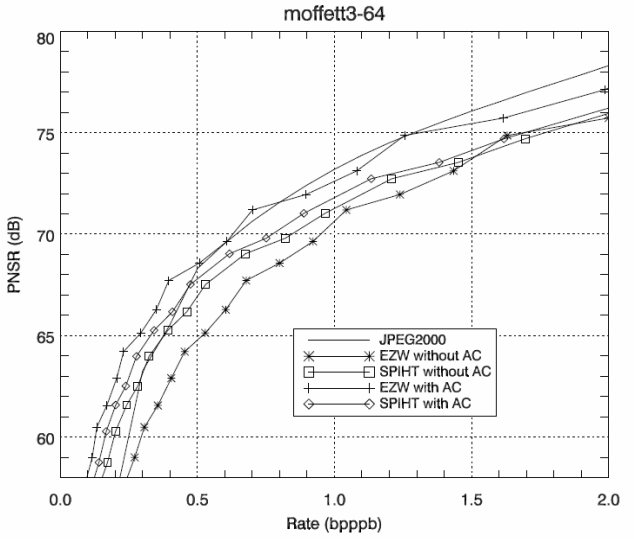

Figure 15: Comparison of compression performances between JPEG2000, EZW and SPIHT with and without arithmetic coder for Moffett3 image (256x256 pixels and 224 bands)

In these referenced papers, only PSNR criterion is shown, but the five criteria defined above as a complete set of representative criteria were also computed. It will be published in a near future.

Lossless performances of 3D-SPIHT-RARS are also presented in 8. In this case, the 5/3 DWT is used instead of the 9/7. JPEG2000 gives lower compression ratio than SPIHT-RARS for hyperspectral images.

4.4.2 ICA results

ICA results are performed for both ICA modified algorithms called ICA_{orth} and ICA_{opt} and are compared with the KLT. These transforms are used as the multicomponent transform in JPEG2000 codec. For clarity, only one example for hyperspectral case is given. PSNR criterion for Cuprite/AVIRIS image is presented Figure 16. KLT and ICA results are very close to each other for all tested hyperspectral images. More precisely, for Jasper and Cuprite images (see Table 3 for Cuprite), ICA performs better than KLT in terms of PSNR value. This is not the case for Moffett image.

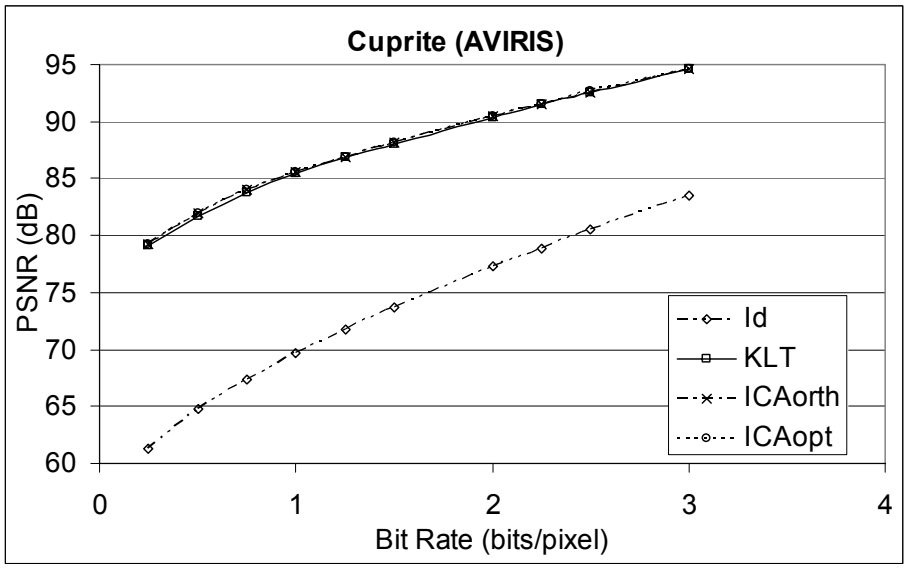

Figure 16: Performances of both ICA algorithms compared to KLT and Identity (no decorrelation) for Cuprite/AVIRIS image (512x512 pixels and 224 bands) for various bit rates.

Table 3: PSNR difference values between ICA algorithms and KLT in dB for each targeted bit rate presented in Figure 16.

Bit Rate (bpp)	**0.25**	**0.5**	**0.75**	**1**	**1.25**	**1.5**	**2**	**2.25**	**2.5**	**3**
ICAorth-KLT	*0.05*	*0.08*	*0.09*	*0.09*	*0.07*	*0.05*	*0.03*	*0.02*	*0.02*	*0.02*
ICAopt-KLT	*0.02*	*0.05*	*0.07*	*0.08*	*0.06*	*0.04*	*0.01*	*0*	*0*	*0*

5 CONCLUSIONS AND FUTURE WORK

In this paper, we have exposed the studies led by CNES in the field of multispectral and hyperspectral image compression. As for the multi-component JPEG2000 standard procedure, CNES has decided to perform a pre-processing stage in order to reduce the correlation in the spectral axis. To do this, several studies have been led by different teams and three algorithms have been proposed: one suited for on-board lossy compression of multispectral images with low complexity and based on a fixed KLT, a second one for hyperspectral data and based on the DWT and a third one based on ICA which could be used for both data types. Whatever the transform, the pre-processing stage allows better compression performances compared to independent compression of each spectral channel. The compression gain is higher for hyperspectral data.

After the pre-processing stage, the transformed data are analyzed by different types of compression schemes depending on the data characteristics to be coded. The fixed KLT is followed by a CCSDS compression and a low-complexity rate allocation procedure. A systematic gain is observed for all test images and the image quality becomes uniform over all bands. Because the algorithm was designed to be adapted to on-board implementation, the quantized model representative of this implementation has performances near to the real model.

The spectral anisotropic DWT is followed by DWT on each band and modified algorithms of EZW and SPIHT adapted to 3D-anisotropic wavelet coefficients. Compared to JPEG2000, those algorithms have very good performances and low complexity. Moreover, their main advantages are: the use of bit plane coding and a fully embedded bitstream output. SPIHT modified algorithm was improved to allow random access to bitstream, a powerful and useful tool for on-board satellite data compression.

The ICA compression scheme is under development but preliminary results show that it is as good as the KLT using JPEG2000 multi-component procedure. Hopefully performances will be of great interest with an adapted zero-tree coding stage after the spatial 2D-DWT.

Results presented in this paper are only statistical quality criteria and performances of the proposed algorithms are mainly driven by Root Mean Square Error value analysis. These studies should be completed with application-related criteria as it was done for hyperspectral data and also visual analyses from experts.

In terms of on-board implementation, the multispectral compression based on a fixed KLT is well adapted. Complexity analyses have been done and an FPGA performing decorrelation, converting and rate allocation procedure is under development. Finally, this FPGA will be used in front of a CCSDS chip simulating the CCSDS compressor. Contrary to both other studies, this first one was really targeted to a spatial implementation. The 3D-SPIHT and 3D-EZW SPIHT algorithms complexity analysis will be done in a near future.

ICA studies for compression is an on-going work. After founding a fixed matrix and proving that its performances are close to the optimal, analysis of a zero-tree coding algorithm will be done. Moreover, the complexity of the ICA method will be studied and a possibility of complexity reduction will be experimented. Another way to apply ICA is also to look for a unique transform for both spatial and spectral correlation reduction. Indeed, although ICA and DWT are good decorrelators for respectively spectral and spatial domains, it does not prove that their association is an optimal for multispectral and hyperspectral redundancy.

REFERENCES

1. C. Thiebaut et al., "On-Board Compression Algorithm for Satellite Multispectral Images", *in Proc. of Data Compression Conference 2006*, Snowbird, March 28-30, 2006.
2. E. Christophe. "Compression des images hyperspectrales et son impact sur la qualité des données". *PhD Thesis École Nationale Supérieure de l'Aéronautique et de l'Espace*, October 2006. (in French)
3. D. S. Taubman and M. W. Marcellin, JPEG2000, *Image compression fundamentals*, standards and practice. Kluwer Academic Publishers (2004).
4. ISO/IEC 15444-2, "Information technology -- JPEG 2000 image coding system: Extensions", 2004
5. Klimesh M., “Low-complexity adaptive lossless compression of hyperspectral imagery”, *in Proc. of the SPIE, Satellite Data Compression, Communications, and Archiving II* , Volume 6300, pp. 63000N (2006).
6. Qian, S.E., “Hyperspectral data compression using a fast vector quantization algorithm”, *IEEE Trans. Geoscience and Remote Sensing*, Vol. 42, Issue 8, p 1791-1798, Aug. 2004.
7. P-S. Yeh et al. , "The New CCSDS Image Compression Recommendation," *in Proc. 2005 IEEE Aerospace Conference*, pp. 1–8, Big Sky, MT, March 5–12, 2005.
8. C. Lambert-Nebout et al., “On-board optical image compression for future high resolution remote sensing systems”, *Proc. SPIE Vol. 4115, Applications of Digital Image Processing XXII*I, Andrew G. Tescher; Ed., December 2000, pp 332-346.
9. E. Christophe, C. Mailhes and P. Duhamel, “Best anisotropic 3-D wavelet decomposition in a rate-distortion sense”, *In Proc. of Int. Conf. on Acoustics and Speech Processing ICASSP’06*, vol. 2, p. II-17-II-20, IEEE, Toulouse, France, May 2006.
10. http://www.kakadusoftware.com/
11. E. Christophe and W. A. Pearlman, “Three-dimensional SPIHT coding of hyperspectral images with random access and resolution scalability”, *in Proc. of Fortieth Annual Asilomar Conference on Signals, Systems and Computers*, Oct. 2006.
12. E. Christophe, P. Duhamel, and C. Mailhes, “Adaptation of Zerotrees Using Signed Binary Digit Representations for 3D Image Coding”, *EURASIP Journal on Image and Video Processing*, vol. 2007, Article ID 54679, 7 pages, 2007.
13. M. Narozny and M. Barret, "ICA-based algorithms applied to image coding*", in Proc. of ICASSP'07*, Page(s): I-1033-I-1036, Honolulu, Hawaii, USA, April 2007.
14. D.-T. Pham, “Fast Algorithms for Mutual Information Based Independent Component Analysis”, *IEEE Transactions on Signal Processing*, Vol. 52 No. 10 (2004).
15. I. P. Akam Bita, M. Barret and D.T. Pham, “Compression of multicomponent satellite images using independent component analysis”, in *Proc. of ICA’06*, pp. 335–342, Charleston (USA), 5-8 March 2006.
16. JPEG2000 Verification Model 9.1 (Technical description), ISO/IEC JTC 1/SC 29/WG 1WG1 N2165, June 2001.
17. E. Christophe, D. Léger and C. Mailhes, “Quality criteria benchmark for hyperspectral imagery”, *IEEE Trans. on Geoscience and Remote Sensing*, vol. 43, Issue 9, p. 2103-2114, Sept. 2005.